International Journal of Thermal Sciences 96 (2015) 227–235

Contents lists available at ScienceDirect

International Journal of Thermal Sciences

journal homepage: www.elsevier.com/locate/ijts

Review

Energy design for dense neighborhoods: One heat pump rejects heat, the other absorbs heat from the same loop

A. Almerbati [a], S. Lorente [b], A. Bejan [a, *]

[a] Duke University, Department of Mechanical Engineering and Material Science, Durham, NC 27708-0300, USA
[b] University of Toulouse, INSA, 135 Avenue de Rangueil, 31077 Toulouse, France

ARTICLE INFO

Article history:
Received 3 November 2014
Received in revised form
21 May 2015
Accepted 22 May 2015
Available online 26 June 2015

Keywords:
Energy
Urban design
Dense neighborhoods
Heat pumps
Ground heat exchangers

ABSTRACT

This paper documents the joint performance of heat pumps that are served by a common loop buried in the ground, and which operate simultaneously: one heat pump absorbs heat from the buried loop whereas the other one rejects heat. A background flow is circulated in the underground loop even when the two heat pumps are not operating. The objective is to determine the performance and the manner in which it is affected by the way in which the two heat pumps are connected to the loop. The performance measures are the heat transfer rates into and out of the heat pumps, and the total pumping power required by the assembly. The paper documents the individual performance of the heat pumps, and their relative performance, which is the ratio of heating absorbed by one pump to the heating rejected by the other pump.

1. Introduction

Ground coupled heat pumps draw heat from and reject heat to the ground, depending on diurnal and seasonal conditions and geographic orientation of the building. Even on the same day and in the same neighborhood, a building facing the sun may need cooling, while a neighboring building facing away from the sun may need heating. The thermal coupling between the heat pump flow system and the ground is influenced by a buried loop through which the heat pump fluid circulates. Heat pumps that provide cooling to the building reject heat to the loop and the ground. Heat pumps that heat the building extract heat from the loop and the ground.

This is an active field of research. Specifically, ground heat exchangers can work in open or closed loops. Here we focus on the closed loop design, which consists of a stream flowing in buried pipes installed horizontally or vertically in the available terrain [1–7]. Ground heat exchangers are traditionally designed as single pipes or channels with arrays of loops or serpentines [6–11]. Closely related to this field, and with impact on a greater scale, is the extraction from geothermal energy from shallow subsurface flow loops. The state of the art in this domain is presented by Vienken et al. [12]. Optimization methods for such designs are described by de Paly et al. [13], Bayer et al. [14] and Daróczy et al. [15]. The energy policy significance of this field is outlined by Hähnlein et al. [16].

The growth of thickly settled neighborhoods pushes the ground coupled design toward multiple heat pumps that are served by the same loop buried in a shared land area. When the heat pumps operate in unison—all rejecting, or all absorbing—the design challenge is to accommodate all the heat pumps by using the same loop. As the density of urban settlement increases further, the multiple heat pump assembly acquires a new feature: some heat pumps reject heat to the ground while at the same time neighboring heat pumps absorb heat from the ground. In this paper we focus on this feature of thickly settled design, and analyze the simultaneous operation and performance of heat pumps that reject and absorb heat from the ground. The simplest such design is shown in Figs. 1–4.

2. Model

We chose the simplest possible model in order to highlight the goal of this work, which is to discover the relationship between the flow configuration and the performance of the combination of two heat pumps. To begin with, we assumed that the heat

* Corresponding author.
E-mail address: abejan@duke.edu (A. Bejan).

http://dx.doi.org/10.1016/j.ijthermalsci.2015.05.007
1290-0729/

Nomenclature

c_{turb}	factor, Eq. (28)
c_P	specific heat of the fluid, J kg^{-1} K^{-1}
D	diameter of the buried pipe, m
f	friction factor for flow in pipe
h	conduction equivalent heat transfer coefficient, W m^{-2} K^{-1}
L	length of duct, m
$\dot{m}_0$	background mass flow rate, kg s^{-1}
$\dot{m}_a$	total mass flow rate through the T_a pipe, kg s^{-1}
$\dot{m}_b$	total mass flow rate through the T_b pipe, kg s^{-1}
$\dot{m}_H$	mass flow rate of HT pump, kg s^{-1}
$\dot{m}_L$	mass flow rate of LT pump, kg s^{-1}
N	number of heat transfer units for the buried pipe
p	perimeter of duct, m
P	pressure, Pa
q_H	heat rejected by HT pump, W
q_L	heat absorbed by LT pump, W
r	mass flow rate ratio, $\dot{m}_L/\dot{m}_H$
r_H	mass flow rate ratio, $\dot{m}_0/\dot{m}_H$
r_L	mass flow rate ratio, $\dot{m}_0/\dot{m}_L$
T_H	high temperature, K
$T_{H,end}$	fluid temperature at the end of T_a pipe (Figs. 2 and 3), K
$T_{H,in}$	temperature of fluid which enters the loop from HT pump, K
$T_{H,out}$	temperature of fluid that exits the loop toward HT pump, K
T_L	low temperature, K
$T_{L,end}$	fluid temperature at the end of T_b pipe (Figs. 3 and 4), K
$T_{L,in}$	temperature of fluid which enters the loop from LT pump, K
$T_{L,out}$	temperature of fluid that exits the loop toward LT pump, K
T_∞	soil temperature, K

Greek symbols

ΔP	pressure difference, Pa
ΔT	temperature difference, K
ε	dimensionless factor, Eq. (8)
ρ	density, kg m^{-3}
τ	dimensionless temperature difference, Eq. (17)

Subscripts

HT	high temperature heat pump
in	inflow
LT	low temperature heat pump
out	outflow

exchanger loop is horizontal (subsurface), not in a vertical hole, even though in high density neighborhoods the available ground area is scarce. An infinite medium is assumed: the effect of the boundaries of the round area is neglected, and so are the diurnal and seasonal temperature trends of the surroundings.

Two heat pumps operate with heat transfer to and from a single-loop heat exchanger buried in the ground. The soil is modeled as a homogeneous solid with constant, uniform and isotropic properties. The thermal resistance of the wall of the buried pipe is assumed negligible relative to the thermal resistance posed by the solid around the pipe. This heat transfer model [16] is discussed further in conjunction with Fig. 6.

The two heat pumps are situated at the opposite ends of the loop. The high temperature heat pump (HT) rejects heat and is located at x = 0, where x is measured along the loop. The low temperature heat pump (LT) absorbs heat and is located at x = L. The objective of the work described in this paper is to identify the design (the flow configuration) such that the overall performance (q_H, q_L) is increased.

In the absence of the heat pumps, an auxiliary pump circulates fluid with the flow rate $\dot{m}_0$ in the clockwise sense shown in the figure. There are four ways to connect the pumps relative to one another. In Fig. 1 mixing occurs downstream of each heat pump. The LT pump draws its stream ($\dot{m}_L$) from the stream that comes from the outlet of the HT pump, namely $\dot{m}_a = \dot{m}_0 + \dot{m}_H + \dot{m}_L$. Right after this connection, the LT pump rejects its $\dot{m}_L$ stream to the loop, so that along the returning leg of the loop the flow rate is $\dot{m}_b = \dot{m}_a$.

In Fig. 2, the order in which the connections of the LT pump are made is reversed. First, the LT pump rejects its $\dot{m}_L$ stream (T_L) to the loop, and then it draws it back at a higher temperature, $T_{L,out}$. Mixing occurs downstream of HT, and upstream of LT. The flow rates in the long ducts of the loop are the same, $\dot{m}_a = \dot{m}_b = \dot{m}_0 + \dot{m}_H$.

The new feature of the design shown in Fig. 3 is that the background $\dot{m}_0$ is the only flow present in the two long stretches of the loop. The LT and HT pumps reject their streams ($\dot{m}_L$, $\dot{m}_H$) to the loop and extract them almost immediately, after the mixing with background flow with higher temperature $T_{L,end}$ and lower Temperature $T_{H,end}$.

The fourth possible way to connect the two heat pumps to the same loop is shown in Fig. 4. New relative to the other configurations is that the circulating fluid through the long legs of the loop contains the background flow $\dot{m}_0$ and the flow rate $\dot{m}_L$. The HT pump flow rate $\dot{m}_H$ enters the loop with T_H and then is extracted after the mixing with lower temperature $T_{H,end}$. Mixing occurs upstream of HT and downstream of LT.

The shape of the loop is not important as long as the ground volume affected by heat transfer with the loop has a thermal penetration distance that is much smaller than the loop length L. The two legs of the loop are in counterflow. They have the same length (L) because when placed in such a counterflow the two legs require a single trench in which to be buried, regardless of the shape of the counterflow, Fig. 5. If the two legs are independent (L_1, L_2) then the total trench length would be greater, $L_1 + L_2$, as shown in the lower part of Fig. 5.

In the design of Fig. 1, the HT pump adds fluid of temperature T_H and mass flow rate $\dot{m}_H$ to the loop. The LT pump adds cold fluid of temperature T_L and mass flow rate $\dot{m}_L$ to the same loop. The heat transfer from the loop to the ground is time dependent, in accord with the solutions for transient heat conduction from a buried cylinder in an infinite isothermal medium [17]. This process can be modeled as heat transfer from a cylinder to an isothermal conducting medium through a heat transfer coefficient h that decreases monotonically in time, Fig. 6. The loop has two long sections. On the warm side (a), the mass flow rate is $\dot{m}_a$ and the fluid changes from $T_{H,in}$ to $T_{L,out}$. On the cold side (b), the flow $\dot{m}_b$ is from $T_{L,in}$ to $T_{H,out}$. The objective of the analysis is the relationship between the heat rejected by one heat pump and the heat absorbed by the other,

$$q_H = \dot{m}_H c_P (T_H - T_{H,out}) \tag{1}$$

$$q_L = \dot{m}_L c_P (T_{L,out} - T_L) \tag{2}$$

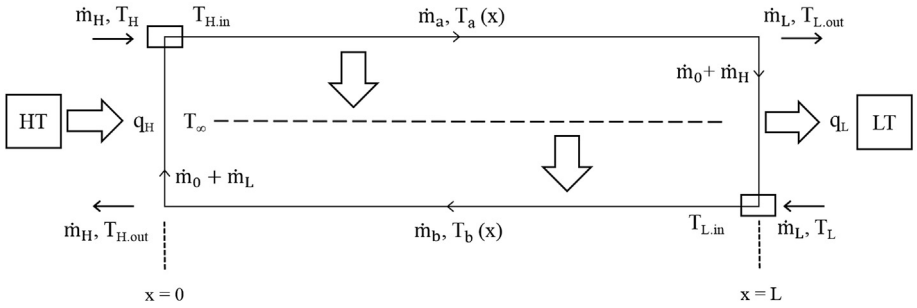

Fig. 1. Two heat pumps on the same loop (HT, LT), one rejecting heat and the other absorbing heat: mixing occurs downstream of each heat pump.

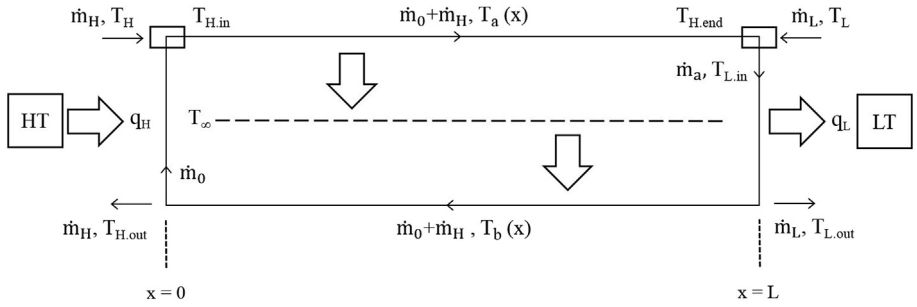

Fig. 2. Two heat pumps on the same loop: mixing downstream of HT, and upstream of LT.

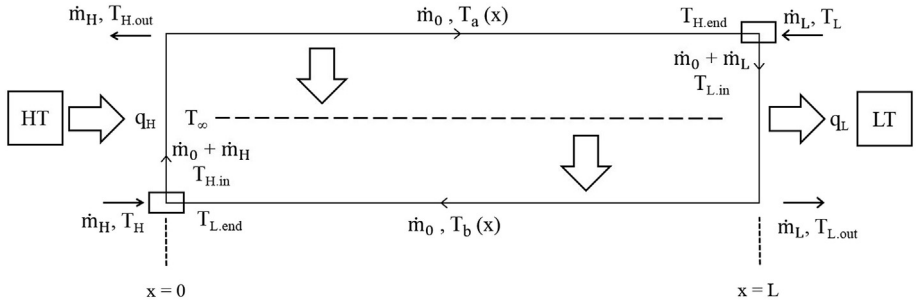

Fig. 3. Two heat pumps on the same loop: mixing upstream of both HT and LT.

When the ratio q_H/q_L is known, the designer knows the relative size of LT vs HT, i.e., how to match the two heat pumps that are served by the same loop. The conservation of mass requires

$$\dot{m}_a = \dot{m}_H + \dot{m}_L + \dot{m}_0 = \dot{m}_b \tag{3}$$

The conservation of enthalpy at the two inlet corners of the loop requires

$$\dot{m}_H c_P T_H + (\dot{m}_0+\dot{m}_L) c_P T_{H,out} = (\dot{m}_0+\dot{m}_H+\dot{m}_L) c_P T_{H,in} \tag{4}$$

$$\dot{m}_L c_P T_L + (\dot{m}_0 + \dot{m}_H) c_P T_{L,out} = (\dot{m}_0 + \dot{m}_H + \dot{m}_L) c_P T_{L,in} \tag{5}$$

Next, the T_a stream is cooled by contact with the ground of uniform far-field temperature T_∞.

The temperature drop along the (a) leg is [18]:

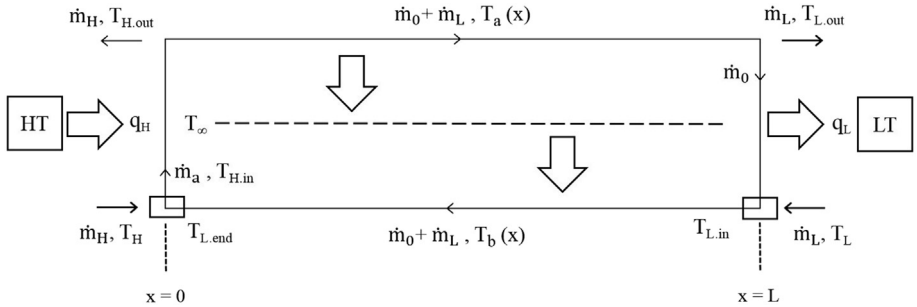

Fig. 4. Two heat pumps on the same loop: mixing upstream of HT and downstream of LT.

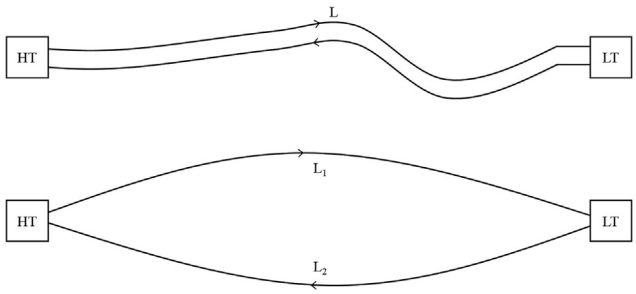

Fig. 5. Slender loop for connecting the two heat pumps in a shorter trench.

$$T_{L,out} - T_\infty = (T_{H,in} - T_\infty)e^{-N} \tag{6}$$

where N is the number of heat transfer units of the buried pipe of length L,

$$N = \frac{h\ p\ L}{\dot{m}_a c_P} \tag{7}$$

p is the perimeter of contact between the T_a pipe and the ground, and h is the conduction-equivalent heat transfer coefficient. Likewise, the T_b stream is heated by contact with the T_∞ ground, and it experiences the temperature rise:

$$T_\infty - T_{H,out} = (T_\infty - T_{L,in})e^{-N} \tag{8}$$

where N is the same as in Eq. (7). The factor e^{-N} accounts for the lifetime of the loop heat transfer process. As the time increases, h decreases (from infinity at $t = 0$), and so does N. This means that e^{-N} increases from zero at $t = 0$, to values that approach 1 as the time increases. The factor e^{-N} marks the passing of time, as shown in Fig. 6. In the remaining analysis, we use the notation $\varepsilon = e^{-N}$ with the observation $\varepsilon < 1$.

3. Results

The objective is to determine the ratio (q_L/q_H) for the four configurations, which from Eqs. (1) and (2) is

$$\frac{q_L}{q_H} = \frac{r_H}{r_L} \cdot \frac{T_{H,out} - T_L}{T_H - T_{L,out}} \tag{9}$$

where

$$r_H = \frac{\dot{m}_0}{\dot{m}_H}, \quad r_L = \frac{\dot{m}_0}{\dot{m}_L}, \quad r = \frac{\dot{m}_L}{\dot{m}_H} \tag{10}$$

For configuration 1, the outlet temperatures ($T_{H,out}$ and $T_{L,out}$) follow from Eqs. (4)–(6) and (8), which can be rewritten as

$$T_H + \left(r_H + \frac{r_H}{r_L}\right)T_{L,out} = \left(1 + r_H + \frac{r_H}{r_L}\right)T_{H,in} \tag{11}$$

$$T_L + \left(r_L + \frac{r_L}{r_H}\right)T_{H,out} = \left(1 + r_L + \frac{r_L}{r_H}\right)T_{L,in} \tag{12}$$

$$T_{L,out} - T_\infty = (T_{H,in} - T_\infty)\varepsilon \tag{13}$$

$$T_\infty - T_{H,out} = (T_\infty - T_{L,in})\varepsilon \tag{14}$$

First, we find that

$$T_{L,out} = (1-\varepsilon)T_\infty + \frac{\varepsilon r_L}{r_L + r_L r_H + r_H}T_H + \frac{\varepsilon(r_H r_L + r_H)}{r_L + r_L r_H + r_H}T_{H,out} \tag{15}$$

$$T_{H,out} = (1-\varepsilon)T_\infty + \frac{\varepsilon r_H}{r_L + r_L r_H + r_H}T_L + \frac{\varepsilon(r_H r_L + r_L)}{r_L + r_L r_H + r_H}T_{L,out} \tag{16}$$

Next, we solve the system (14)–(15) for $T_{H,out}$ and $T_{L,out}$ and introduce the notation

$$T_H = T_\infty + \tau\Delta T \tag{17}$$

$$T_L = T_\infty - (1-\tau)\Delta T \tag{18}$$

where $\Delta T = T_H - T_L$, and τ is a number between 0 and 1, which marks the position of T_∞ between T_H and T_L. The analysis concludes with

$$\frac{T_{L,out} - T_L}{\Delta T} = a_1\tau + b_1(1-\tau) \tag{19}$$

and

$$\frac{T_H - T_{H,out}}{\Delta T} = a_2\tau + b_2(1-\tau) \tag{20}$$

for which the coefficients are listed in the first line of Table 1. The ratio q_L/q_H emerges as a function of mass flow rate imbalance $(\dot{m}_L/\dot{m}_H)$ and time (ε), cf. Eq. (9),

$$\frac{q_L/q_H}{\dot{m}_L/\dot{m}_H} = \frac{a_1\tau + b_1(1-\tau)}{a_2\tau + b_2(1-\tau)} \tag{21}$$

Broadly speaking, q_L/q_H should increase when $\dot{m}_L/\dot{m}_H$ increases: this is why $\dot{m}_L/\dot{m}_H$ is the denominator on the left side of Eq. (21). The right side accounts for the effect of $\dot{m}_L/\dot{m}_H$ and ε on the presumed proportionality between the size ratio q_L/q_H and the ratio of mass flow rates, $\dot{m}_L/\dot{m}_H$. As time increases, ε approaches 1,

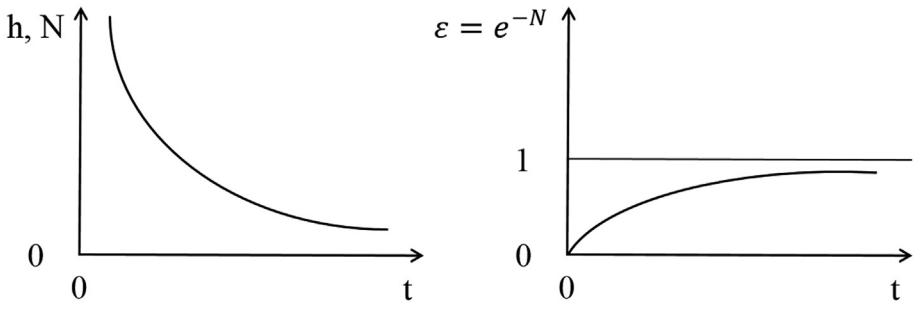

Fig. 6. Why the variable $\varepsilon = e^{-N}$ increases monotonically in time, and marks the direction of time.

Table 1
The coefficients for Eqs. (19) and (20).

Fig. 1	$a_1 = \frac{\varepsilon r_L(r_L + r_L r_H + r_H)}{(r_L + r_L r_H + r_H)^2 - \varepsilon^2(r_H^2 r_L + r_L^2 r_H + r_L^2 r_H^2 + r_L r_H)}$	$a_2 = 1 - \frac{\varepsilon^2(r_L r_H + r_L^2)}{(r_L + r_H r_L + r_H)^2 - \varepsilon^2(r_H^2 r_L^2 + r_L^2 r_H + r_H^2 r_L + r_H r_L)}$
	$b_1 = 1 - \frac{\varepsilon^2(r_H^2 r_L + r_H^2)}{(r_L + r_L r_H + r_H)^2 - \varepsilon^2(r_H^2 r_L + r_L^2 r_H + r_L^2 r_H^2 + r_L r_H)}$	$b_2 = \frac{\varepsilon r_H(r_H + r_H r_L + r_L)}{(r_L + r_H r_L + r_H)^2 - \varepsilon^2(r_H^2 r_L^2 + r_H^2 r_L + r_L^2 r_H + r_H r_L)}$
Fig. 2	$a_1 = \frac{\varepsilon r_L}{r_L + r_L r_H + r_H - \varepsilon^2 r_L r_H}$	$a_2 = 1 - \frac{\varepsilon^2 r_L}{r_L + r_L r_H + r_H - \varepsilon^2 r_L r_H}$
	$b_1 = 1 - \frac{r_H}{r_L + r_L r_H + r_H - \varepsilon^2 r_L r_H}$	$b_2 = \frac{\varepsilon r_H}{r_L + r_L r_H + r_H - \varepsilon^2 r_L r_H}$
Fig. 3	$a_1 = \frac{\varepsilon r_L}{(1 + r_L)(1 + r_H) - \varepsilon^2 r_L r_H}$	$a_2 = 1 - \frac{1 + r_L}{(1 + r_L)(1 + r_H) - \varepsilon^2 r_L r_H}$
	$b_1 = 1 - \frac{1 + r_H}{(1 + r_L)(1 + r_H) - \varepsilon^2 r_L r_H}$	$b_2 = \frac{\varepsilon r_H}{(1 + r_L)(1 + r_H) - \varepsilon^2 r_L r_H}$
Fig. 4	$a_1 = \frac{\varepsilon r_L}{r_L + r_L r_H + r_H - \varepsilon^2 r_L r_H}$	$a_2 = 1 - \frac{r_L}{r_L + r_L r_H + r_H - \varepsilon^2 r_L r_H}$
	$b_1 = 1 - \frac{\varepsilon^2 r_H}{r_L + r_L r_H + r_H - \varepsilon^2 r_L r_H}$	$b_2 = \frac{\varepsilon r_H}{r_L + r_L r_H + r_H - \varepsilon^2 r_L r_H}$

and the right side of Eq. (21) approaches $\dot{m}_H/\dot{m}_L$ which means that q_L/q_H approaches 1. This is confirmed in Fig. 7a, in which we plotted Eq. (25). Generally, the ratio q_L/q_H is smaller than 1, and this means that the LT pump extracts from the ground only a fraction of the energy deposited by the HT pump.

In the limit where $\dot{m}_0$ vanishes, the ratios r_L and r_H approach zero, and the coefficients for Eqs. (19) and (20) reduce to

$$a_1 = \frac{\varepsilon(1+r)}{(1+r)^2 - r\varepsilon^2} \quad b_1 = 1 - \frac{\varepsilon^2 r^2}{(1+r)^2 - r\varepsilon^2} \tag{22}$$

$$a_2 = 1 - \frac{\varepsilon^2}{(1+r)^2 - r\varepsilon^2} \quad b_2 = \frac{\varepsilon r(1+r)}{(1+r)^2 - r\varepsilon^2} \tag{23}$$

where r is the mass flow rate imbalance between the two heat pumps, cf. Eq. (10). Fig. 7b illustrates the effect of the primary flow amount $\dot{m}_0$ which is circulated in the underground loop in the absence of the heat pumps. When $\dot{m}_0$ vanishes, there is a minor decline in the relative performance of the two heat pumps; however, when r_H is raised from 0.1 to 0.5, the relative performance slightly increases. Therefore, the performance of the two heat pump is proportional to $\dot{m}_0$; however, the power needed to the auxiliary pump is also increased.

The analysis of the design of Fig. 2 proceeds along the same steps as in Eqs. (1)–(20). The new coefficients for Eqs. (19) and (20) are listed in the second entry of Table 1. The performance of the two-pump assembly in configuration 2 is illustrated in Fig. 8a. The figure shows that as the time (ε) increases, the ratio q_L/q_H approaches to 1. In addition, the performance q_L/q_H increases significantly with increasing the mass flow rate ratio, $\dot{m}_L/\dot{m}_H$. Fig. 8b shows a remarkable impact in the relative performance of the two heat pumps when $\dot{m}_0$ is changed. For the three ratios, there is an increase in the performance q_L/q_H when the ratio $\dot{m}_L/\dot{m}_H$ increases.

For the design of Fig. 3, the analysis concludes again with Eqs. (19) and (20), for which the coefficients are reported in the third entry of Table 1. Fig. 9a shows the relative performance ratio q_L/q_H changes linearly as the time (ε) increases because $\dot{m}_L$ *and* $\dot{m}_H$ are not pumped through the long buried stretches in which the temperature varies exponentially. When the ratio $\dot{m}_L/\dot{m}_H$ is less than 1, the relative performance increases as time (ε) increases. In contrast, the performance decreases with a time when the ratio $\dot{m}_L/\dot{m}_H$ is greater than 1. The influence of varying $\dot{m}_0$ is shown in Fig. 9b in which q_L/q_H increases as the background stream increases. The heat transfer presence of the underground loop disappears when $\dot{m}_0$ vanishes, because in that limit, $a_1 = b_1 = a_2 = b_2 = 0$.

For the configuration shown in Fig. 4, the analysis produces the coefficients shown in the bottom entry of Table 1, which are to be used in Eqs. (19) and (20). The performance of the two heat pumps is reported in Fig. 10a, which shows that the ratio q_L/q_H decreases, over time, regardless of flow rate ratio r. The relative performance ratio q_L/q_H is significantly larger in Fig. 10a than in Figs. 7a, 8a and 9a. Fig. 10b shows that the ratio q_L/q_H decreases as $\dot{m}_0$ (e.g., r_H) increases, in contrast with the other three configurations.

The analysis of the relative performance between the two heat pumps shows the overall ratio of the heat that could be extracted or rejected to the loop. However, the amount of heat absorbed by the LT pump or rejected by the HT pump from the underground coupled loop is not represented by the relative performance ratio.

To complete the description of the performance of the system, we calculated q_L and q_H and expressed them in dimensionless terms. The reference heat transfer rate was selected as $\dot{m}_H c_P(T_\infty - T_L)$. The dimensionless version of q_L is a function of τ

$$\tilde{q}_L = \frac{\dot{m}_L c_p\ (T_{L,out} - T_L)}{\dot{m}_H c_p (T_\infty - T_L)} = \frac{r\ (T_{L,out} - T_L)}{(1-\tau)(T_H - T_L)} = \frac{r}{(1-\tau)}\ [a_1\tau + b_1(1-\tau)] \tag{24}$$

Similarly, the dimensionless heat current rejected by the HT pump is

$$\tilde{q}_H = \frac{\dot{m}_H c_p\ (T_H - T_{H,out})}{\dot{m}_H c_p\ (T_H - T_\infty)} = \frac{T_H - T_{H,out}}{\tau(T_H - T_L)} = \frac{a_2\tau + b_2(1-\tau)}{\tau} \tag{25}$$

The variation of the dimensionless heat rate for the design of Fig. 1 is shown in Fig. 7c. As the mass flow rate ratio r increases, $\tilde{q}_L$ increases with approximately the same order of r. However, $\tilde{q}_H$ decreases in time (ε) when $r < 1$, and it increases when $r > 1$. Fig. 8c shows that the dimensionless heat transfer rate rejected from the HT pump ($\tilde{q}_H$) is higher than the heat transfer rate gained by the LT pump ($\tilde{q}_L$), despite the increase of ratio $\dot{m}_L/\dot{m}_H$.

In the design of Fig. 3, the heat transfer rates absorbed or rejected to the underground loop are much smaller compared with three other configurations, as shown in Fig. 9c. The variation of $\tilde{q}_H$ and $\tilde{q}_L$ is almost the same as time (ε) increases. Furthermore, as the ratio r increases, the change of $\tilde{q}_L$ is insignificant. Fig. 10c shows that the value of $\tilde{q}_L$ increases over time, until ε reaches to approximately 0.4, and then it decreases. The design of Fig. 4 provides a higher heat transfer rate $\tilde{q}_L$ than the other configurations.

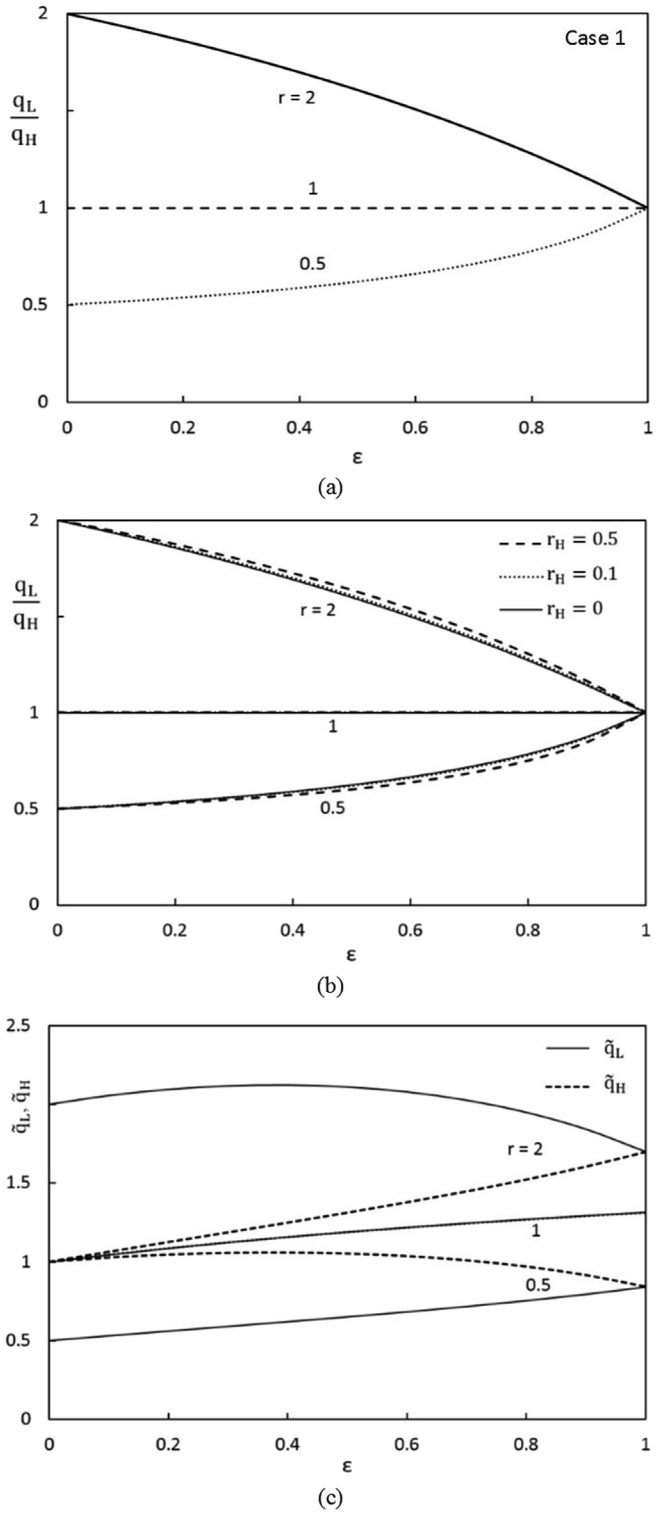

Fig. 7. Results for the design of Fig. 1: (a) the relative performance q_L/q_H of the two heat pumps, (b) the influence of $\dot{m}_0$ on the relative performance and (c) the time variation of the dimensionless heat rates.

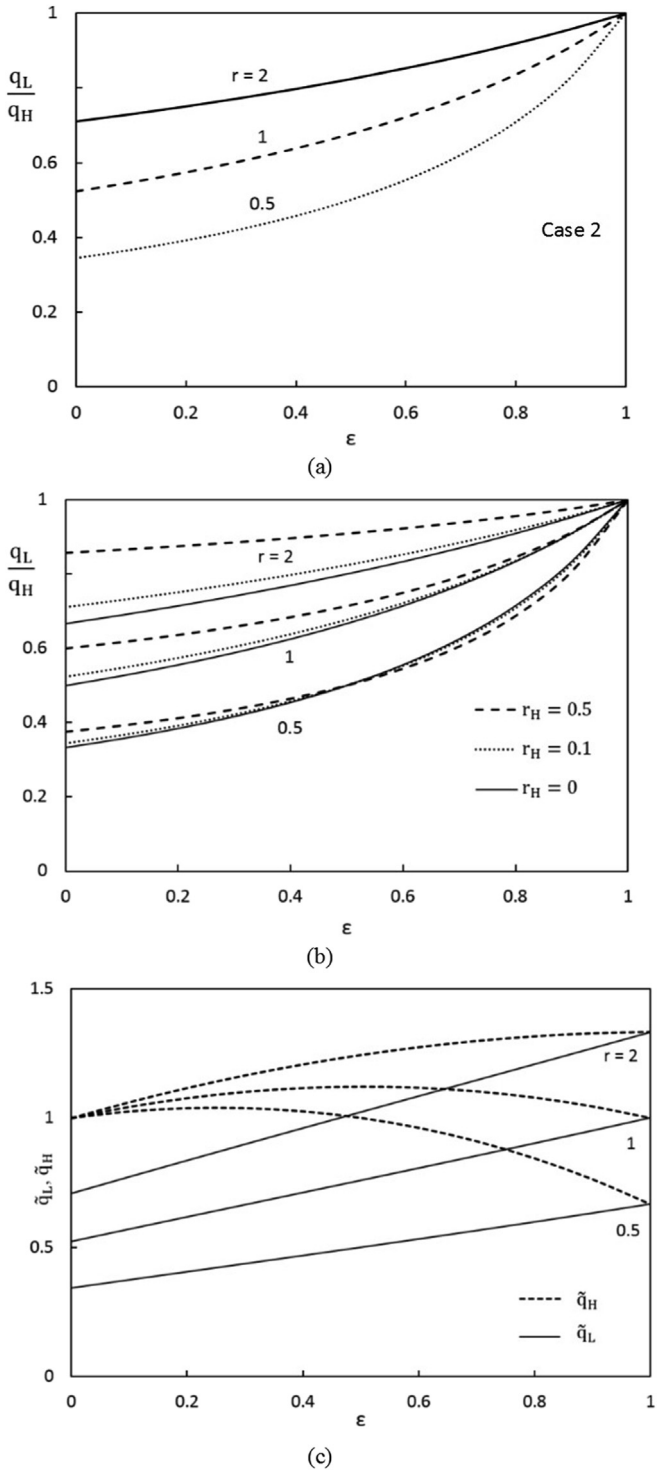

Fig. 8. Results for the design of Fig. 2: (a) the relative performance q_L/q_H of the two heat pumps, (b) the influence of $\dot{m}_0$ on the relative performance and (c) the time variation of the dimensionless heat rates.

4. Pumping power

The analysis of the pumping power required by the underground stream is discussed in this section. We assume that the flow through the buried pipe is in the fully turbulent and fully rough regime such that ΔP is proportional to $\dot{m}^2$,

$$\Delta P = \frac{8f}{\rho}\frac{L}{\pi D^5}\dot{m}^2 \tag{26}$$

The pumping power associated with the pressure difference ΔP and the total length of the duct is

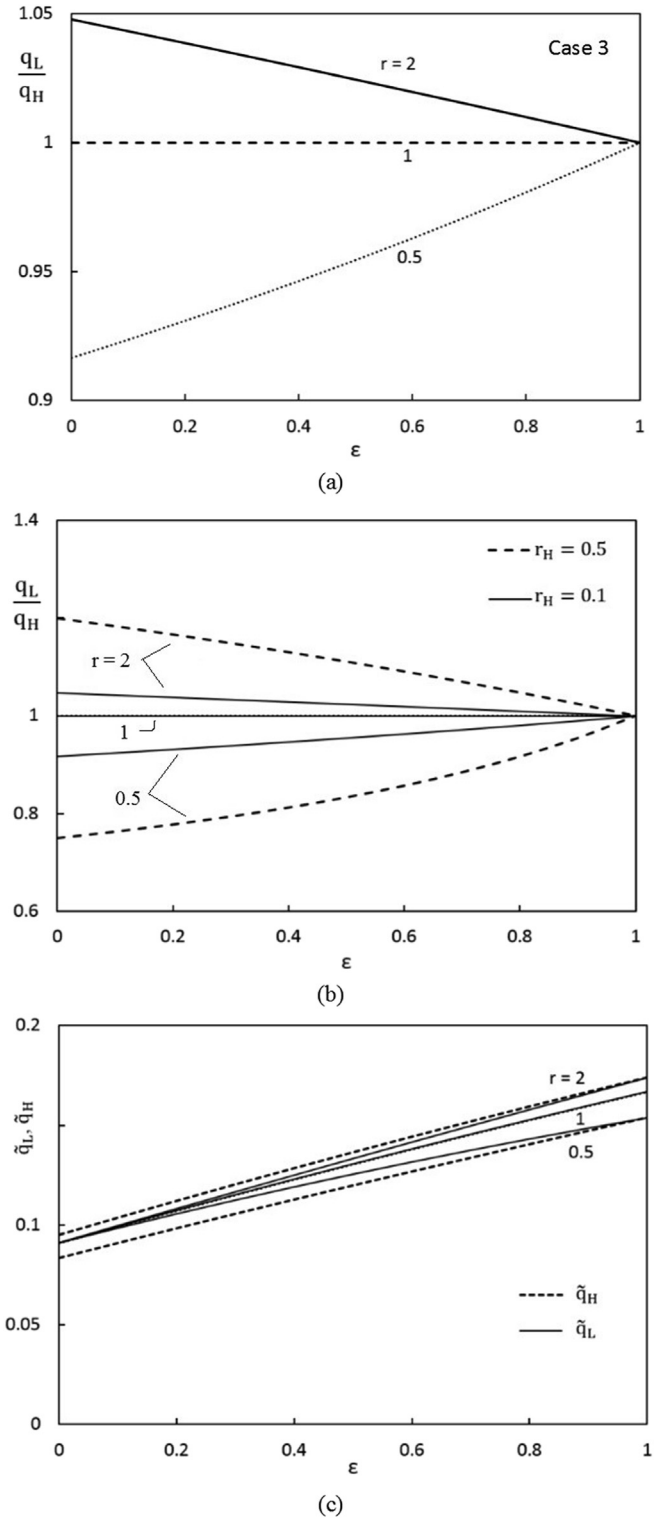

Fig. 9. Results for the design of Fig. 3: (a) the relative performance q_L/q_H of the two heat pumps, (b) the influence of $\dot{m}_0$ on the relative performance and (c) the time variation of the dimensionless heat rates.

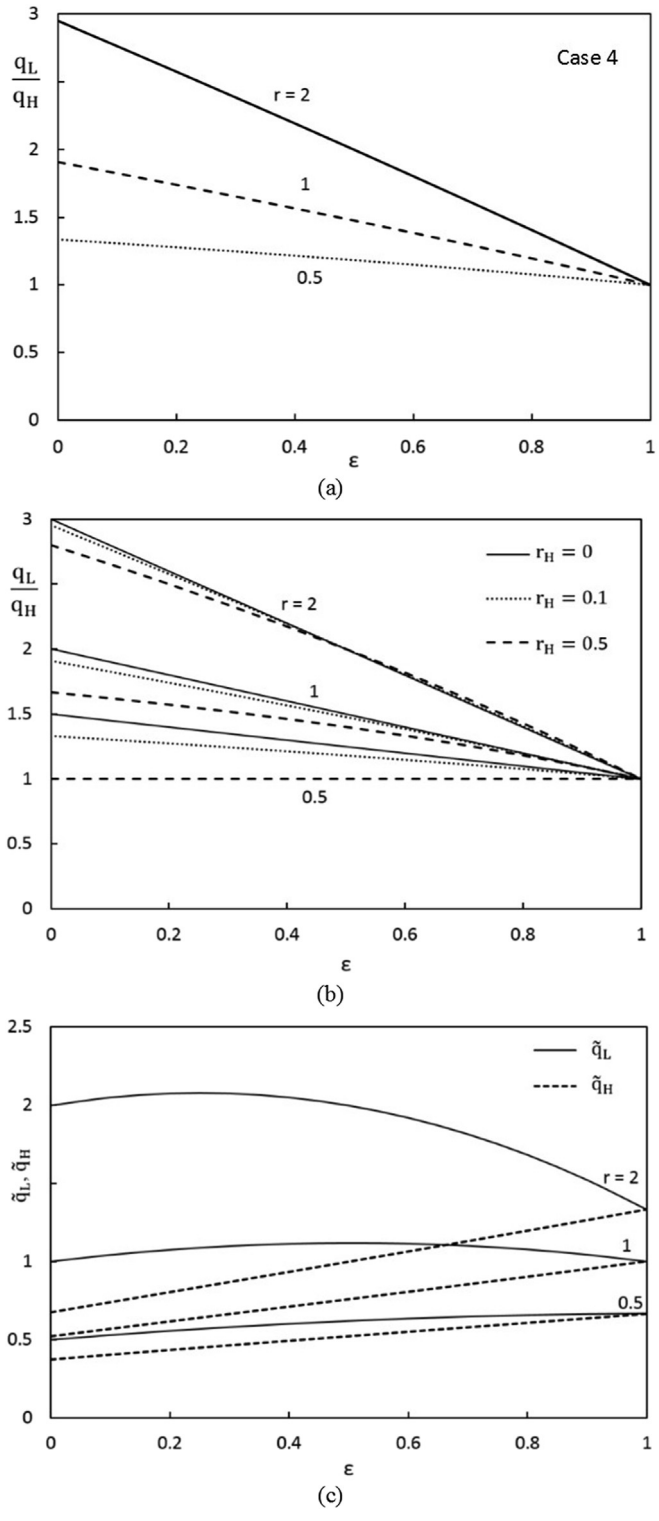

Fig. 10. Results for the design of Fig. 4: (a) the relative performance q_L/q_H of the two heat pumps, (b) the influence of $\dot{m}_0$ on the relative performance and (c) the time variation of the dimensionless heat rate.

$$W = \frac{\dot{m}_a \Delta P_a}{\rho} + \frac{\dot{m}_b \Delta P_b}{\rho} \tag{27}$$

Eqs. (26) and (27) yield

$$W = c_{turb}\dot{m}_a^3 + c_{turb}\dot{m}_b^3 \tag{28}$$

where the constant is $c_{turb} = 8fL/(\rho^2\pi D^5)$. The reference pumping power is based on $\dot{m}_H$, namely $\dot{W}_{ref} = c\dot{m}_H^3$. The dimensionless pumping power is $\tilde{W} = \dot{W}/\dot{W}_{ref}$, which for the designs of Figs. 1–4 become

$$\tilde{W}_1 = \dot{m}_a^3 \Big/ \dot{m}_H^3 = (1 + r_H + r)^3 \tag{29}$$

$$\tilde{W}_2 = (\dot{m}_0 + \dot{m}_H)^3 \Big/ \dot{m}_H^3 = (1 + r_H)^3 \tag{30}$$

$$\tilde{W}_3 = \dot{m}_0^3 \Big/ \dot{m}_H^3 = r_H^3 \tag{31}$$

$$\tilde{W}_4 = (\dot{m}_0 + \dot{m}_L)^3 \Big/ \dot{m}_H^3 = (r_H + r)^3 \tag{32}$$

Fig. 11 shows the variation of the heat current $\tilde{q}_H$ rejected by HT pump as the pumping power and the background mass flow rate increase. For clarity, the ratio $\dot{m}_L/\dot{m}_H$ was set equal to 1, and the time parameter ε was set at 0.2. The four designs divide themselves into two groups. In Figs. 1 and 2, $\tilde{q}_H$, decreases as $\tilde{W}$ increases. In Figs. 3 and 4, the trend is the opposite. In conclusion, to reject more heat and use less power, the superior designs are 1 and 2.

Similarly, in Fig. 12 we plotted the relationship between the heat current absorbed by the LT heat pump and the required pumping power. This time, the four design group themselves differently: only in Figs. 1 and 4 is a greater $\tilde{q}_L$ achievable with less $\tilde{W}$. Together, Figs. 11 and 12 show that only the design of Fig. 1 offers greater $\tilde{q}_H$ and $\tilde{q}_L$ with less $\tilde{W}$.

5. Conclusions

In this paper we documented the merits of a design consisting of two heat pumps buried underground and connected to the single loop-shaped ground heat exchanger. The goal of the work presented in this paper was to discover how the changes in the configuration of the flow system affect the performance of the assembly. We found that if we endow the configuration with freedom to change, and if we compare the resulting alternatives on the same basis, it is possible to identify not only the better configurations but the key design feature that influences the performance. That feature is the position of the mixing process relative to its closest heat pump.

We considered four different ways in which the two heat pumps are connected to the loop. We reported the individual heat transfer rates experienced by the two heat pumps, and the relative performance ratio q_L/q_H. The results show that the best design is the one defined in Fig. 1, where mixing occurs downstream of both LT and

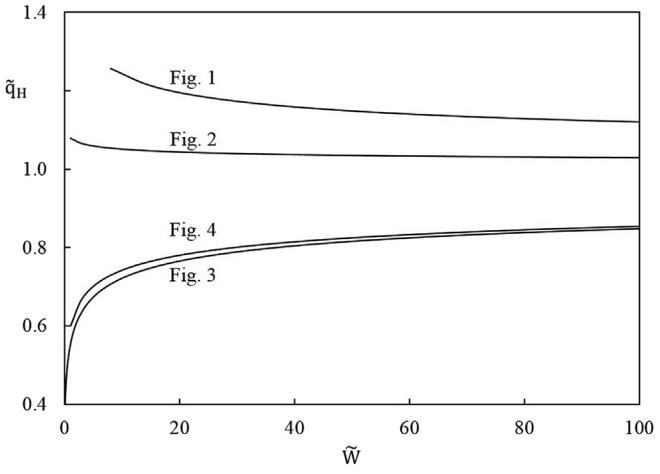

Fig. 11. The effect of the total pumping power on the rate of heat rejection from the HT pump.

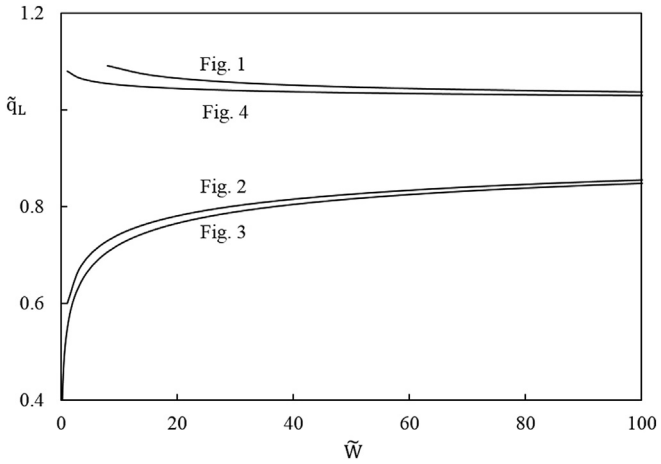

Fig. 12. The effect of the total pumping power on the rate of heat absorption at the LT pump.

HT, in which case a higher heat ($\tilde{q}_H$) could be rejected to the ground and simultaneously absorbed by LT pump ($\tilde{q}_L$). On the other hand, the results for the design of Fig. 2 showed higher capability to reject heat from the HT pump to the underground loop. Specifically, configuration 2 is more applicable when the sole need is to cool a building, while configuration 4 should be used when the need is to heat the neighboring buildings. The effect of the increasing background flow rate $\dot{m}_0$ on the heat gained or rejected to the underground loop was also analyzed. The design of Fig. 4 offers a performance that is superior to the designs of Figs. 1–3, as shown in Figs. 7a, 8a and 9a and 10a.

The implications of the present work are of fundamental character. The conclusion that morphing the flow configuration freely is the key to higher performance is generally applicable, especially in the field of ground-coupled heat pumps for thickly settled urban areas. Future studies may employ the method of this paper in more realistic models that incorporate the features that were neglected in the present model. Options for making the model more realistic are the inclusion of temperature changes in the environment, and boundary effects such as the presence of additional one-loop assemblies in the close proximity of the system analyzed in this paper.

Acknowledgment

Mr. Almerbati's work was supported by King Fahd University of Petroleum and Minerals through the PhD scholarship at Duke University. Prof. Bejan's and Prof. Lorente's work was sponsored by the National Science Foundation.

References

[1] B. Sanner, C. Karytsas, D. Mendrinos, L. Rybach, Current status of ground source heat pumps and underground thermal energy storage in Europe, Geothermics 32 (2003) 579.
[2] H. Demir, A. Koyun, G. Temir, Heat transfer of horizontal parallel pipe ground heat exchanger and experimental verification, Appl. Therm. Eng. 29 (2009) 224.
[3] H. Esen, M. Inalli, M. Esen, Numerical and experimental analysis of a horizontal ground-coupled heat pump system, Build. Environ. 42 (2007) 1126.
[4] H. Esen, M. Inalli, M. Esen, K. Pihtili, Energy and exergy analysis of a ground-coupled heat pump system with two horizontal ground heat exchangers, Build. Environ. 42 (2007) 3606.
[5] K. Woods, A. Ortega, The thermal response of an infinite line of open loop wells for ground coupled heat pump systems, Int. J. Heat. Mass Transf. 54 (2011) 5574.
[6] D. Bozis, K. Papakostas, N. Kyriakis, On the evaluation of design parameters effects on the heat transfer efficiency of energy piles, Energy Build. 43 (2011) 1020.

[7] T. Katsura, K. Nagano, S. Takeda, Method of calculation of the ground temperature for multiple ground heat exchangers, Appl. Therm. Eng. 28 (2008) 1995.
[8] Y. Yang, M. Li, Short-time performance of composite-medium line-source model for predicting response of ground heat exchangers with single U-shaped tube, Int. J. Therm. Sci. 82 (2014) 130.
[9] J. Darkwa, G. Kokogiannakis, C.L. Magadzire, K. Yuan, Theoretical and practical evaluation of an earth-tube (E-tube) ventilation system, Energy Build. 43 (2011) 728.
[10] V. Khalajzadeh, G. Heidarinejad, J. Srebric, Parameters optimization of a vertical ground heat exchanger based on response surface methodology, Energy Build. 43 (2011) 1288.
[11] J. Vaz, M.A. Sattler, E.D. Dos Santos, L.A. Isoldi, Experimental and numerical analysis of an earth-air heat exchanger, Energy Build. 53 (2011) 2476.
[12] T. Vienken, S. Schelenz, K. Rink, P. Dietrich, Sustainable intensive thermal use of the shallow subsurface—a critical view of the status quo, Groundwater 53 (2014) 356.
[13] M. de Paly, J. Hecht-Méndez, M. Beck, P. Blum, A. Zell, P. Bayer, Optimization of energy extraction for closed shallow geothermal systems using linear programming, Geothermics 43 (2012) 57.
[14] P. Bayer, M. de Paly, M. Beck, Strategic optimization of bore hole heat exchanger field for seasonal geothermal heating and cooling, Appl. Energy 136 (2014) 445.
[15] L. Daróczy, G. Janiga, D. Thévenin, Systematic analysis of the heat exchanger arrangement problem using multi-objective genetic optimization, Energy 65 (2014) 364.
[16] S. Hähnlein, P. Bayer, G. Ferguson, P. Blum, Sustainability and policy for the thermal use of shallow geothermal energy, Energy Policy 59 (2013) 914.
[17] M.R. Errera, S. Lorente, R. Anderson, A. Bejan, One underground heat exchanger for multiple heat pumps, Int. J. Heat. Mass Trans. 65 (2013) 727.
[18] A. Bejan, Convection Heat Transfer, fourth ed., Wiley, Hoboken, 2013.